

RESEARCH ARTICLE | AUGUST 22 2025

Damping and vibration properties of alginate–poloxamer hydrogels doped with sepiolite and cactus fibers

Gianni Comandini ; Fabrizio Scarpa  ; Evita Ning; Graham J. Day ; Hesam Ramezani ;
James P. K. Armstrong ; Abderrezak Bezazi ; Adam W. Perriman 



APL Mater. 13, 081122 (2025)

<https://doi.org/10.1063/5.0280619>



Articles You May Be Interested In

Investigating various polymers as candidates of in situ gelformers for Ketotifen delivery

AIP Conf. Proc. (February 2023)

The effect of sepiolite loading on curing and tensile properties of sepiolite filled natural rubber/styrene-butadiene rubber (SMR L/SBR) blends

AIP Conf. Proc. (September 2020)

Influence of intumescent flame retardant and sepiolite on the mechanical and rheological behavior of polypropylene

AIP Conf. Proc. (May 2016)



APL Materials

Now Online: Roadmap articles

AIP
Publishing

Read Now

Damping and vibration properties of alginate-poloxamer hydrogels doped with sepiolite and cactus fibers

Cite as: APL Mater. 13, 081122 (2025); doi: [10.1063/5.0280619](https://doi.org/10.1063/5.0280619)

Submitted: 13 May 2025 • Accepted: 5 August 2025 •

Published Online: 22 August 2025



View Online



Export Citation



CrossMark

Gianni Comandini,¹ Fabrizio Scarpa,^{1,a)} Evita Ning,² Graham J. Day,^{2,3} Hesam Ramezani,¹ James P. K. Armstrong,⁴ Abderrezak Bezazi,⁵ and Adam W. Perriman^{2,6}

AFFILIATIONS

¹ Bristol Composites Institute, School of Civil, Aerospace and Design Engineering (CADE), University of Bristol, Bristol BS8 1TR, United Kingdom

² School of Cellular and Molecular Medicine, University of Bristol, Bristol BS8 1TD, United Kingdom

³ Centre for the Cellular Microenvironment, Division of Biomedical Engineering, James Watt School of Engineering, The Advance Research Centre, University of Glasgow, Glasgow G12 8QQ, United Kingdom

⁴ Translational Health Sciences, Bristol Medical School, University of Bristol, Bristol BS1 3NY, United Kingdom

⁵ Laboratoire de Mécanique Appliquée des Nouveaux Matériaux, Université 8 Mai 1945, Guelma, Algeria

⁶ Research School of Chemistry and John Curtin School of Medical Research, Australian National University, Canberra, ACT 2601, Australia

^{a)}Author to whom correspondence should be addressed: f.scarpa@bristol.ac.uk

ABSTRACT

We investigated a novel class of composite hydrogels composed of alginate, poloxamer, sepiolite, and cactus fibers for vibration damping applications. Using a design of experiments methodology, we systematically correlated manufacturing parameters with mechanical and damping properties, using dynamic mechanical analysis and vibration testing. The hydrogels were characterized under controlled temperature, frequency, and humidity conditions, with results demonstrating that the storage modulus can reach up to twice that of pure hydrogel formulations using diluted dispersions with total additive concentration below 2 wt %. Sepiolite additions below 0.3 wt % were found to stabilize the material response to temperature variations, while cactus fibers enhanced both stiffness and damping performance in a concentration-dependent manner. Optimal performance was achieved with a formulation containing 5 wt % alginate, 5 wt % poloxamer, 0.1 wt % sepiolite, and 2 wt % cactus fibers. This composition provided a favorable balance between quasi-static mechanical integrity and dynamic damping capability, with loss factors exceeding 0.4. These findings provide a foundation for developing advanced and sustainable hydrogel materials with tailororable vibration damping characteristics.

© 2025 Author(s). All article content, except where otherwise noted, is licensed under a Creative Commons Attribution (CC BY) license (<https://creativecommons.org/licenses/by/4.0/>). <https://doi.org/10.1063/5.0280619>

I. INTRODUCTION

Vibration and acoustic damping technologies have a long history, with references and device designs for vibration mitigation found in the works of Lord Rayleigh,¹ Bishop,² and Kolsky.³ Vibration and damping treatments were also developed in the early 1940s by both Allied and Axis forces.^{4,5} However, the designs of passive vibration, thermal, and acoustic insulators have changed little

since the introduction of multi-layer insulators and polymeric constrained/free layer dampers in the early 1960s, which are used to stabilize cooling systems and manage flutter-type and acoustically radiating vibrations in aircraft, helicopters, and marine structures. Damping and energy dissipation performance of free and constrained layers dampers depend on their architecture and on the viscoelasticity of their polymers, with varying storage and damping ($\tan \delta$) based on temperature–frequency equivalence via Arrhenius

or Williams–Landel–Ferry relations.⁶ Typical elastomers used for these damping technologies have moduli varying between 5 MPa and 2.6 GPa when passing from a rubbery to glass state. Soft polymers that are mostly used in constrained layer dampers have moduli varying between 170 kPa and 100 MPa between 90 and –37 °C, with damping (loss) factors of ~0.9 at 25 °C.⁴ When used within vibrating composite beams, the overall loss factors of the system, however, drop to ~0.3.⁷ At a constant temperature, the higher the excitation frequency provided by the dynamic load, the more the polymer approaches the glassy state and becomes dynamically rigid, resulting in a loss factor decrease.

Most of the materials used in the current state-of-the-art damping and absorption technologies are based on manipulation of synthetic chemistry and are fundamentally fossil-like in nature. Bio-based materials, however, provide an alternative to fossil-based solutions. Natural fibers (flax, hemp, and wood) have tan δ/damping loss factors between 8% and 20% when embedded within thermoplastics and thermoset composites (PLA and epoxies), with the relative humidity increasing the damping by 50% when passing from 20% to 80% of relative humidity.⁸ Hydrogels⁹ can also be produced using bio-based and biodegradable sources and offer some interesting behavior in terms of damping capacity. Recoverable energy dissipation from drop tower impact tests has been observed in sodium alginate–silicon nitride PVA composite biomaterials.¹⁰ Lead zirconate titanate (PZT)–polydimethylsiloxane (PDMS) gels have shown loss factors of ~20% within 1–20 Hz sweeps performed with dynamic mechanical analyzers.¹¹ Wang *et al.* analyzed polyacrylamide (PAAm) and PDMS gels using a bending rig with base acceleration. PAAm gels had viscous damping ratios of ~2%–3%, while PDMS beams showed ratios around 8%.¹² Polyurethane–carbon nanotube–PDMS gel composites have shown loss factors exceeding 24% in vibration transmissibility tests between 50 and 600 Hz.¹³ Hydrogels based on PVA and alginate–poloxamer can also be used as a platform to host reinforcing natural fibers, such as flax.¹⁴ Diluted dispersions of flax fibers provide increased stiffness and strength and higher water absorption capability but lower thermal stability compared to other natural fiber reinforcements such as jute. Another class of natural fiber reinforcements is represented by cactus. Cactus fibers are derived from sheaths of *Opuntia ficus-indica* (prickly pear). The plant is native and endemic to the Mediterranean region, North Africa, Latin America, Australia, and Texas, where it is commonly used as feed for cattle.¹⁵ The fibers have shown to exhibit multi-scale fractal geometry characteristics that enhance stick–slip friction and bonding to the matrix.^{16–18} Slip–stick friction effects have also been demonstrated from preliminary vibration transmissibility tests on alginate–poloxamer gels up to 5.0 wt %.¹⁹ Nanoclays constitute, however, a more widespread type of reinforcement in hydrogel composites. Sepiolite ($\text{Si}_{12}\text{O}_{30}\text{Mg}_8(\text{OH})_4(\text{H}_2\text{O})_4\cdot\text{H}_2\text{O}$) is a particularly interesting type of nanoclay formed by precipitation of near-surface brackish or saline waters under semi-arid climatic conditions.²⁰ The special structure of the sepiolite generates nanofillers with a large aspect ratio and high surface area for significant sorption capability. In addition, the negative surface charge of sepiolite allows strong complexation with positively charged polymers or surfaces. These properties have been used to develop layer-by-layer coatings with polymers such as chitosan and poly(acrylic) acid (PAA) to enhance the vibration damping, dynamic stiffness, and impact energy absorption in foams and other porous materials used for

packaging.^{21,22} Sepiolite is considered one of the most efficient nanoclay fillers to produce environmentally sustainable hydrogel systems for retaining water and dyes,²³ antibacterial and self-healing properties,²⁴ and a significant increase in storage moduli and loss factors has been observed during shear rheology tests.^{25,26}

Recent work²⁷ has demonstrated that alginate–poloxamer hydrogels form tunable porosity architectures and can achieve dynamic moduli over ~2.5 MPa and loss factors between ~15% and 28% within the 80–300 Hz frequency range under vibration transmissibility tests. Bio-printed cactus microfiber-doped alginate–poloxamer hydrogel monoliths¹⁸ when subjected to vibration excitation also tend to increase the dynamic modulus of almost an order of magnitude compared to their static moduli and loss factors between ~18% and 30%. The cactus provides a stiffening effect at low concentrations; however, the synergy between slip–stick effects provided by the fractal cactus fibers¹⁶ and the alginate–poloxamer networks generates an ~1 order of magnitude increase in the dynamic modulus between 50 and 150 Hz under vibration.¹⁹ To provide an indication of the significance of these numbers, state-of-the-art polyurethane foams used for energy absorption/packing show a maximum increase in the dynamic modulus of 50% when compared to the static modulus of ~100 kPa due to the stiffening poroelastic effect provided by the gas trapped within the tortuous foam skeleton.²⁸ However—to the best of our knowledge—no data are available about the viscoelasticity and vibration damping performance of alginate–poloxamer hydrogel composites containing sepiolite reinforcements, or combined sepiolite/natural fiber cactus fillers. Overall, there is a significant gap in our understanding of how various types of nanoclays and natural fiber reinforcements contribute to the quasi-static and dynamic performance of bio-based and sustainable hydrogels, such as alginate–poloxamer.

This work describes a systematic design of experiments (DoE) campaign to assess the quasi-static, viscoelastic, and vibration transmissibility properties of novel alginate–poloxamer hydrogels reinforced by sepiolite and cactus fiber reinforcements. A fractional factorial design involving 53 different experiments has been carried out to assess storage and loss moduli with dynamic mechanical analysis (DMA), and loss factors and dynamic modulus via vibration transmissibility tests. Significantly, the DMA tests are carried out at constant relative humidity levels (20% RH) to avoid effects from lack/acquisition of moisture from the environment.

II. DESIGN OF EXPERIMENTS (DOE) AND MATERIALS

The materials involved in this design of experiments are poloxamer, alginate, sepiolite, and cactus fibers. The alginate–poloxamer base of the hydrogels was kept constant at 5 wt % alginate and 5 wt % poloxamer, following the optimal baseline composition identified in Ref. 19. A design of experiments methodology was implemented following a fractional factorial design approach.²⁹ The cactus fibers used in this work have been ball-milled with a cryomill (zirconium balls); the resulting fibers had average thickness dimensions between 2.5 and 3 μm . Poloxamer 407 was incorporated into the hydrogel formulation to regulate the gelation temperature, improving both injectability and the practical usability of the material. By maintaining a constant concentration of 5 wt %

TABLE I. Summary of hydrogel samples prepared with varying weight percentages of sodium alginate, poloxamer 407, sepiolite, and cactus fibers.

Sample type	Sodium alginate (wt. %)	Poloxamer 407 (wt. %)	Sepiolite (wt. %)	Cactus fibers (wt. %)	Replicates
1	5	5	0	0	2
2	5	5	0.1	0	4
3	5	5	0.3	0	6
4	5	5	0.5	0	3
5	5	5	0.1	0.5	5
6	5	5	0.1	1	4
7	5	5	0.1	2	4
8	5	5	0.3	0.5	5
9	5	5	0.3	1	2
10	5	5	0.3	2	2
11	5	5	0.5	0.5	4
12	5	5	0.5	1	2
13	5	5	0.5	2	2
14	5	5	0	0.5	2
15	5	5	0	1	2
16	5	5	0	2	4

across all samples, we standardized their thermo-responsive behavior, ensuring a consistent influence on gelation and mechanical properties. Sodium alginate was also included in the formulation as a constant component, maintained at a 5 wt %.¹⁹ The 5 wt % alginate–poloxamer was also previously identified as the hydrogel configuration offering the best trade-off in terms of quasi-static mechanical properties and vibration damping.²⁷ Weight fractions between 0.1% and 0.5% of sepiolite have previously shown to provide a significant increase in loss modulus in chitosan²¹ and PAA-based²² nanocoatings deposited on open cell polyurethane foams. Weight fractions of cactus fibers between 0.5% and 2% have also shown in the previous generation of alginate–poloxamer–cactus fiber composites the best trade-off in terms of stiffness and energy absorption.¹⁹

The fractional factorial design resulted in a total of 16 replicated experimental conditions for a total of 53 experiments (Table I).

Samples used for vibration transmissibility tests had one replicate only.

A 12.5% w/w poloxamer 407 solution was prepared by gradually dissolving 2.5 g poloxamer 407 into 20 g precooled deionized water (diH₂O at 4 °C) under continuous stirring, maintaining the temperature throughout. Mixing continued until a homogeneous, clear solution was obtained. Poloxamer 407 is thermo-responsive, remaining in a liquid state below 10–15 °C and undergoing gelation above 30–37 °C. Gel formation was induced by incubating the solution at 37 °C. Separately, a 12.5% w/w sodium alginate solution was prepared by dissolving 2.5 g of sodium alginate in 20 g of diH₂O. The two solutions were subsequently combined to yield a uniform composite mixture. To achieve a final target mass of 50 g, an additional 10 g of deionized water was initially intended for inclusion. However, when sepiolite and/or cactus fibers were incorporated as additives, their respective masses were subtracted from this 10 g allocation to maintain a constant total mass. The resulting mixtures were subjected to three mixing cycles at 2500 rpm for 5 min each, with 15 min rest intervals between cycles, ensuring thorough homogenization and degassing. The blended formulations were then cast into molds and enclosed within dialysis membranes. These encapsulated samples were immersed in a 2 L bath of diH₂O containing 147.01 g of calcium chloride (500 mM) at 37 °C for 24 h to induce Ca²⁺-mediated alginate cross-linking. Following gelation, the hydrogels were removed from the dialysis membranes and stored in 1 L of diH₂O supplemented with 14.7 g of calcium chloride (100 mM) to preserve structural integrity before further testing.

III. TESTING METHODS

Microstructures of the gels were analyzed using cryo-scanning electron microscopy (Quanta 200 with Field Emission Gun and Gatan Alto 2500 Cryo-SEM attachment). The composition of the gels was evaluated via infrared spectrometry using a PerkinElmer Spectrum 100 with a resolution of 1 cm⁻¹ and scans between 4000 and 500 cm⁻¹. The viscoelastic properties of the composite hydrogels were evaluated using a Dynamic Mechanical Analysis facility (DMA 850 from Texas Instruments). Tests were performed in a relative humidity (RH) chamber maintained at constant 20% RH, a value substantially lower than the standard ambient level of ~50%

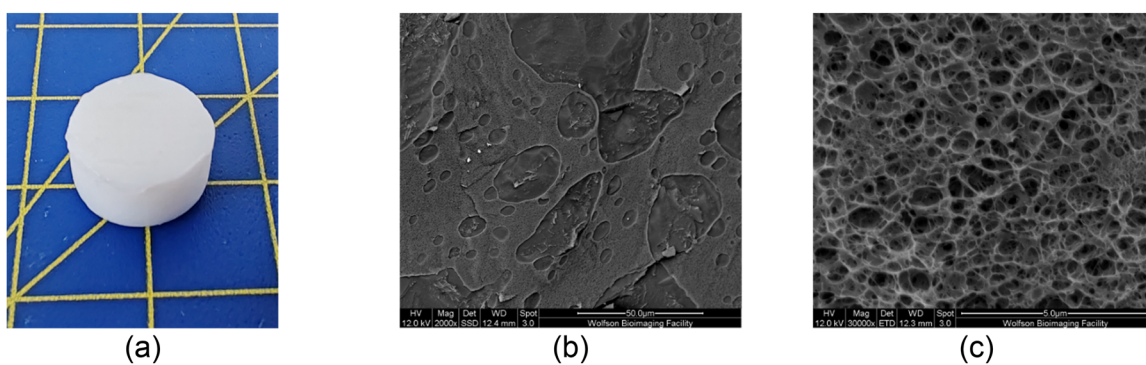


FIG. 1. (a) Alginate–poloxamer 5 wt. % cross-linked with CaCl₂ prepared for DMA testing within an environmental chamber. Cryo-SEM images of the microstructure at different magnifications [(b) and (c)], illustrating the porogen-based architecture of the hydrogels.

at standard room temperatures. The samples were mounted using a submersion clamp and subjected to cyclic compression loading at 1 Hz, a frequency commonly used to evaluate the viscoelastic response of hydrogels.^{10,30} The temperature was varied between 3 and 95 °C; however, only data up to 60 °C were retained for analysis. This temperature range was selected to evaluate the thermal stability and performance of the hydrogels under conditions exceeding physiological incubation temperature. Notably, the gels exhibited significant compression and dimensional reduction (by a factor of 3) after repeated harmonic cycling, especially at temperatures above 70 °C. This deformation results in a stiffening response, which is evident from the increase in the measured modulus. For this

purpose, we considered data only up to a maximum compressive strain of 10% to extract properties near the linear elastic regime in the viscoelasticity of hyperelastic polymers.³¹

Vibration transmissibility tests have been carried out to determine the dynamic modulus and loss factors²⁸ of the hydrogels within frequency ranges from 80 to 180 Hz at room temperature. The specimens used for the vibration transmissibility tests were dimensioned at 30 × 30 × 15 mm³. The experimental protocol involved evaluating these specimens under four distinct top mass conditions: 74.9, 121.6, 168.6, and 239.2 g. These masses were affixed to the upper plate, while the hydrogel samples were affixed to the upper and lower plates. A DEHP Alginate Tray Adhesive Liquid was used to ensure

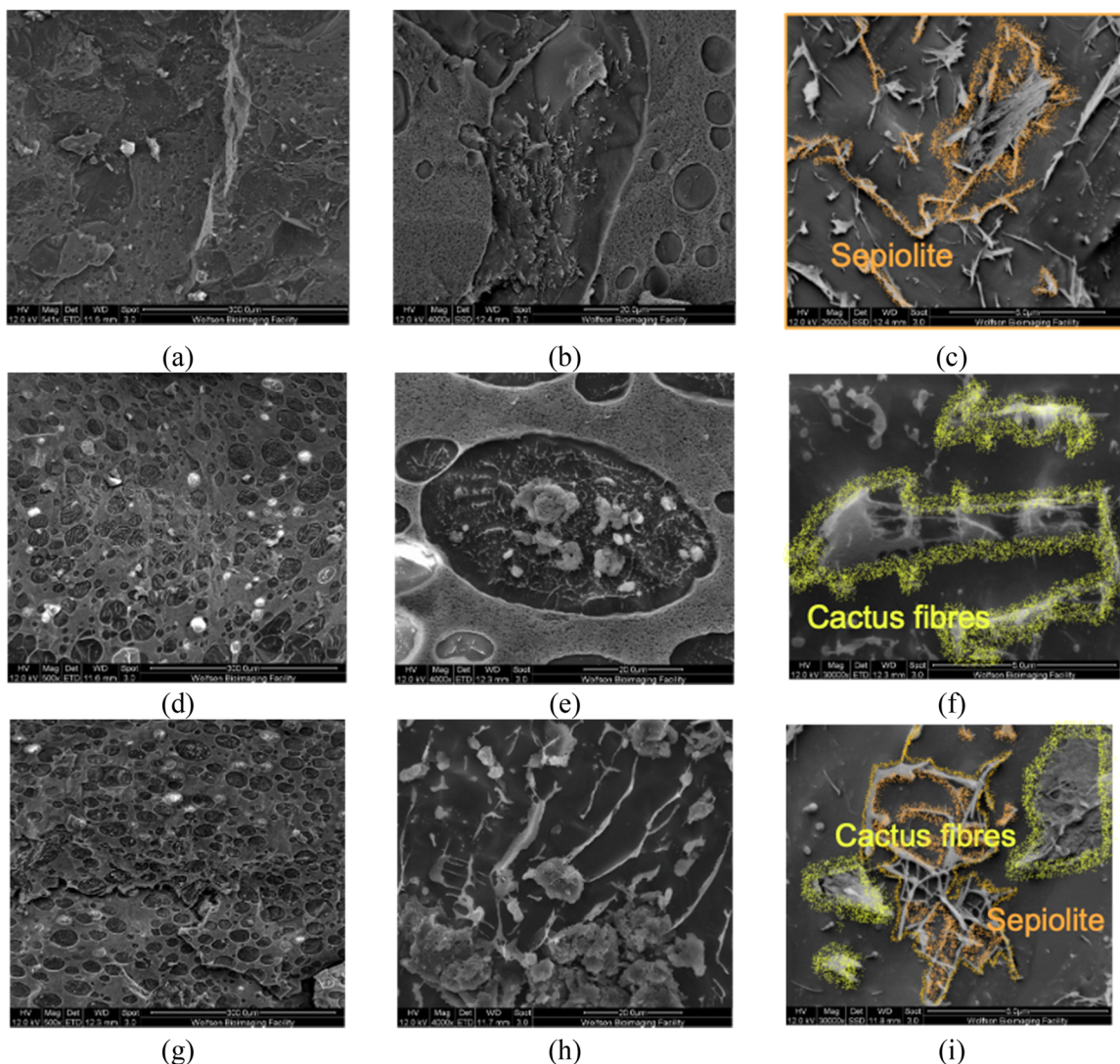


FIG. 2. Cryo-SEM images of the microstructures of the composite hydrogels at 300 μm [(a), (d), and (g)], 20 μm [(b), (e), and (h)], and 5 μm [(c), (f), and (i)] details of magnification. (a)–(c) Composites with 0.3 wt. % of sepiolite reinforcement, (d)–(f) composites with cactus reinforcement only at 2 wt. %, and (g)–(i) samples with sepiolite 0.1 wt. % and cactus at 1 wt. %. Cactus fiber and sepiolite reinforcements are artificially contoured in green and orange, respectively.

secure contact between the plates and the sample. The lower plate was connected to an electrodynamic shaker (LDS, Model V406), which delivered controlled vibrational excitation. To quantify the vibration transmission, two accelerometers (PCB, Model 333M07) were mounted to measure acceleration at both the base and upper plates. Each test consisted of two cycles, with each cycle consisting of five 10-s segments. During each segment, white noise was applied at different energy levels, resulting in a total test excitation time of 50 s per cycle. A 10-s interval between cycles was introduced to allow for system stabilization. The root mean square acceleration applied to the base plate was controlled and set to values of 4.6, 7.6, 12.0, 17.9, and 22.5 m/s^2 .

IV. RESULTS

A. Microstructure of the composite hydrogels

The baseline alginate–poloxamer hydrogel showed the presence of a structured 3D network, with pore diameters ranging from ~ 1.3 to $15 \mu\text{m}$ (Fig. 1). These dimensions are consistent with the porogenic effect induced using poloxamer.²⁷ The incorporation of the sepiolite and cactus fiber reinforcements alters the microstructure of the composite hydrogels (Fig. 2). Both sepiolite and cactus fibers appear to form good interfacial bonding with the alginate–poloxamer matrix. The rough surface texture of the cactus fiber [Fig. 2(f)] enhances the bonding to the matrix and the load transfer during mechanical loading.¹⁷

The FTIR spectra of the three types of composites hydrogels in Fig. 2 and the baseline poloxamer–sodium alginate gel are shown in Fig. 3. Sodium alginate has peaks at 3000 , 2850 , 1596 , 1412 , 1297 , and 1081 to 1027 cm^{-1} , attributing to stretching vibrations of OH, stretching vibrations of CH, antisymmetric CO_2 stretching, symmetric stretching of CO_2 , skeletal vibrations of the backbone, and antisymmetric stretching of C–O–C, respectively.³² For poloxamer 407, the main characteristic peaks are located at 3467 , 2889 , 1671 , and 1110 cm^{-1} , attributing to OH stretching, aliphatic CH stretching, CH_2 bending, and C–O stretching vibrations, respectively.³³ The characteristic peaks for sepiolite are observed at 3689 , 3574 , 3419 , 1663 , 1449 , 1209 , 1023 , 785 , and 645 cm^{-1} . These correspond to various vibrations and bonds: OH stretching, Mg–OH stretching, water molecule stretching and bending, carbonate impurities, Si–O–Si bonding, in-plane Si–O–Si vibrations, and Mg–OH bending (for 785 and 645 cm^{-1}).³⁴ The characteristic peaks for cactus fibers typically appear as follows: 2895 to 2915 cm^{-1} for C–H stretching vibrations, 1680 to 1750 cm^{-1} for carbonyl groups, 1600 to 1634 cm^{-1} for aromatic C=C stretching in lignin, 1375 to 1500 cm^{-1} for C–H and symmetric CH_3 bending, and 1000 to 1300 cm^{-1} for C–O group vibrations.^{16,35} In general, the FTIR spectra are dominated by organic bonds associated with calcium alginate and poloxamer: 3236 cm^{-1} (OH stretching), 1594 cm^{-1} (asymmetric C=O stretching in calcium coordinated alginate carboxylate), 1418 cm^{-1} (symmetric C=O stretching in calcium coordinated alginate and C–H bending), 1299 cm^{-1} (skeletal vibrations of the backbone), 1028 , 1081 , 1128 , and 1145 cm^{-1} (C–O stretching in the poloxamer aliphatic ether and alginate alcohol), and 820 – 890 cm^{-1} (C–H bending of the alginate ring). These signals overlapped with the organic bonds present in the cactus fiber samples; however, there was a faint peak at 614 cm^{-1} in the sepiolite samples, which may be attributable to bending vibrations of Mg–OH.

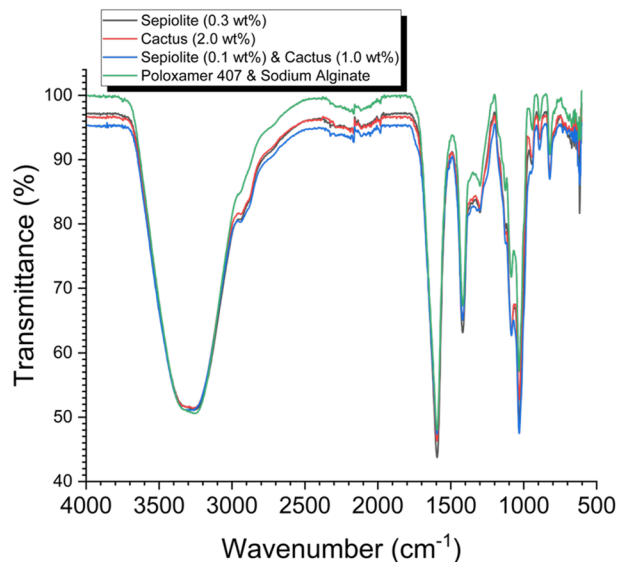


FIG. 3. FTIR of the hydrogel composites with 0.3 wt. % of sepiolite reinforcement, with cactus reinforcement at 2 wt. %, and with sepiolite at 0.1 wt. % and cactus at 1 wt. %. Baseline correction was performed using the poloxamer and sodium alginate values at 4000 cm^{-1} .

B. Quasi-static DMA tests

Figure 4 displays the overall loss modulus curves vs temperature for a subset of the gels tested within the design of experiments. Peaks of loss modulus for the different hydrogel composites occurred between ~ 75 and 95°C . Loss moduli tended to feature a low sensitivity vs temperature within the ~ 25 – 60°C range, with a steep increase of up to ~ 3 orders of magnitude when approaching

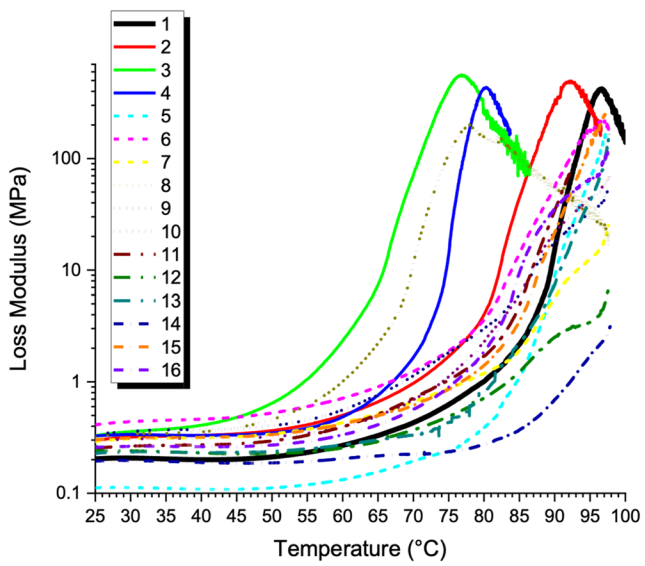


FIG. 4. Example of loss modulus curves between 25 and 100°C of all the samples tested with the DMA at 1 Hz and 20% RH.

the peak of the loss modulus. A more detailed comparison at the distribution of the storage and loss moduli for the different combinations of hydrogels at 30, 45, and 60 °C is shown in Fig. 5. The baseline alginate–poloxamer gels exhibited stable values of storage and loss moduli across these three different temperatures (~1.2 and ~0.22 MPa, respectively). The deviations in the storage modulus at 30 °C ranged from 5% of the mean value for sample no. 14 (0 wt. % sepiolite and 0.5 wt. % cactus) to ~60% for sample no. 12 [0.5 wt. % sepiolite and 1 wt. % cactus, Fig. 5(a)]. The deviations, however, increased with the increasing testing temperature. This was evident for sample no. 6 (0.1 wt. % sepiolite and 1 wt. % cactus), with deviations ~90% for storage and loss moduli at 60 °C. Notably, alginate–poloxamer gels are primarily designed for tissue engineering applications at 37 °C, where their structural integrity and material homogeneity are optimal. The energy absorption (loss modulus) of the 0.3 wt. % sepiolite was the largest at 60 °C (0.7 MPa), although variability was substantial with a high deviation. This likely reflects reduced structural integrity at elevated temperature, which compromises the microstructure of the undoped gel. The gels with 0.1 wt. % sepiolite and 1 wt. % cactus also exhibited considerable loss moduli at 30 and 45 °C (~0.37–0.6 MPa). While the standard deviations remain high at 60 °C, they were lower than for 0.3 wt. %

sepiolite samples. Notably, 0.3 wt. % sepiolite and 1 wt. % cactus fiber formulations showed relatively low standard deviations and consistent energy absorption values ranging from 0.3 MPa at 30 °C to 0.55 MPa at 60 °C.

C. Vibration transmissibility tests

Figure 6 shows the cumulative transfer function plots from the vibration transmissibility tests conducted on various gel systems. The resonance frequencies are generally clustered between 80 and 140 Hz. Minor peaks in the transfer function are observed around 40 Hz; however, these are attributed to slight rocking motions of the gel/top mass system, likely caused by minor eccentricities in the dynamic load. The very small amplitude of this rocking resonance does not appear to affect the primary uniaxial/compressional dynamic characteristics measured during the vibration transmissibility tests.

The distributions of dynamic moduli, loss factors, and resonant frequencies for the different gels' formulations are shown in Fig. 7. Within the 80–150 Hz range, the highest loss modulus values were observed in gels containing 0.1 wt. % sepiolite and up to 2.0 wt. % cactus, reaching 0.32 MPa. The corresponding dynamic

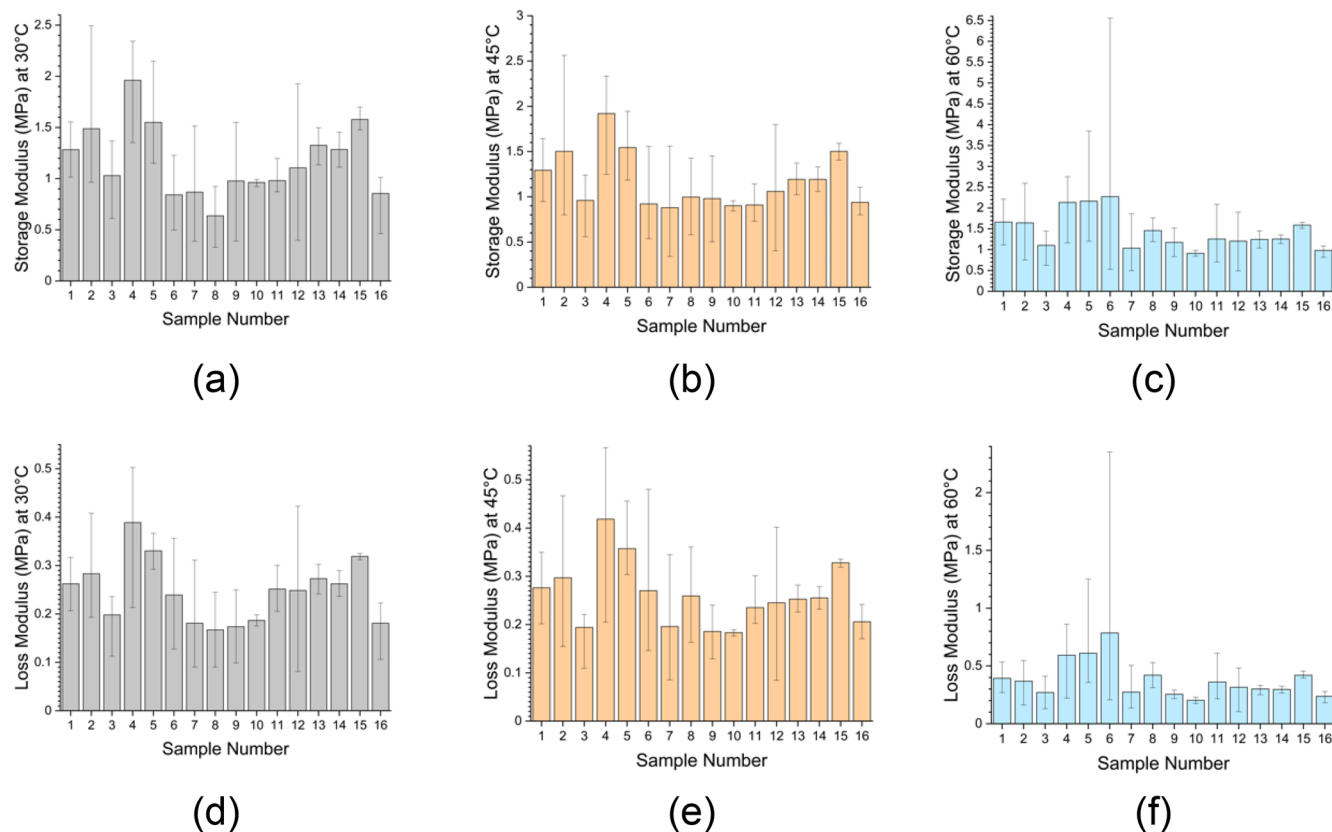


FIG. 5. Distributions of the storage moduli [(a)–(c)] and loss moduli [(d)–(f)] of the different classes of composite hydrogels. (a) and (d) values measured at 30 °C, (b) and (e) values measured at 45 °C, and (c) and (f) values measured at 60 °C. Bars indicate deviations within each sample replicates.

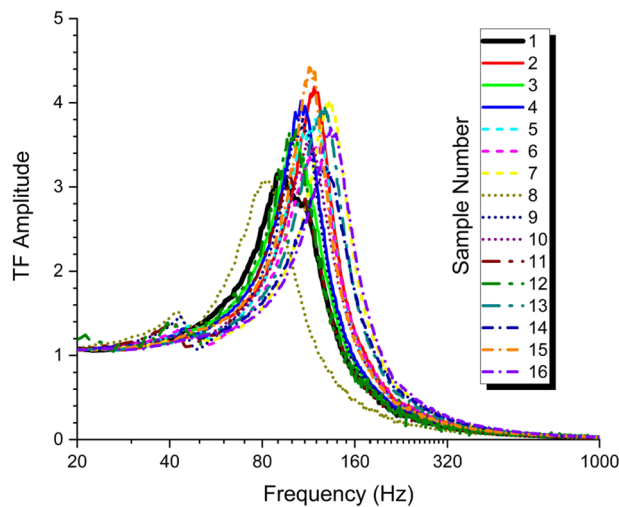


FIG. 6. Distribution of the transmissibility curves for the different types of composite hydrogel samples measured at room temperature.

modulus for this configuration is 0.93 MPa. Notably, gels with 0.5 and 1.0 wt. % cactus fibers exhibited similar loss modulus values around 0.3 MPa, indicating a plateau in energy dissipation performance at these intermediate concentrations. Increasing the sepiolite concentration beyond 0.1 wt. % does not result in higher dynamic or loss modulus values; instead, a reduction of 10%–20% was observed compared to the 0.1 wt. % sepiolite formulation. However, increasing the cactus fiber content appeared to enhance the performance at a constant weight fraction of sepiolite. For instance, in gels with

0.3 wt. % sepiolite, the loss modulus increased monotonically from 0.18 MPa with cactus at 0.5 wt. % to 0.27 MPa at 2.0 wt. %. This positive trend with increasing cactus fiber reinforcement was consistent across all sepiolite weight fractions investigated.

V. DISCUSSION

A. Role of sepiolite

Previous studies using mechanical testing and shear rheology have demonstrated that incorporating 10 wt. % of sepiolite into polyvinyl alcohol (PVA) composite gels can increase toughness by a factor of 60 and enhance the loss modulus at 10 Hz and 25 °C by 50%, respectively.²⁵ Higher sepiolite concentrations (20–40 wt. %) in castor-oil gel-like dispersions have similarly resulted in a 5000-fold increase in the loss modulus.²⁶ Furthermore, sepiolite has been shown to maintain thermal and chemical stability in paraffin composites subjected to over 200 thermal cycles in differential scanning calorimetry experiments.³⁶ In the present study, a notable increase in storage and loss modulus at 1 Hz was observed in alginate–poloxamer gels with only 0.1 wt. % sepiolite. However, when the sepiolite concentration exceeds 0.3 wt. %, the reinforcement effect diminishes. This reduction is attributed to the clustering of sepiolite particles within the matrix, which inhibits effective load transfer between the sepiolite and the alginate–poloxamer matrix, thereby compromising the mechanical performance. A similar trend is observed in the dynamic and loss moduli identified using the vibration transmissibility testing, with the effect being more pronounced at high temperatures. For instance, the 0.3 wt. % sepiolite gels increased their loss modulus from 0.27 MPa at 30 °C to 0.7 MPa at 60 °C. Comparable trends are observed at lower sepiolite concentrations (0.1 wt. %) and when 1 wt. % cactus fibers are incorporated, with the loss modulus increasing from ~0.4 MPa at 30 °C to

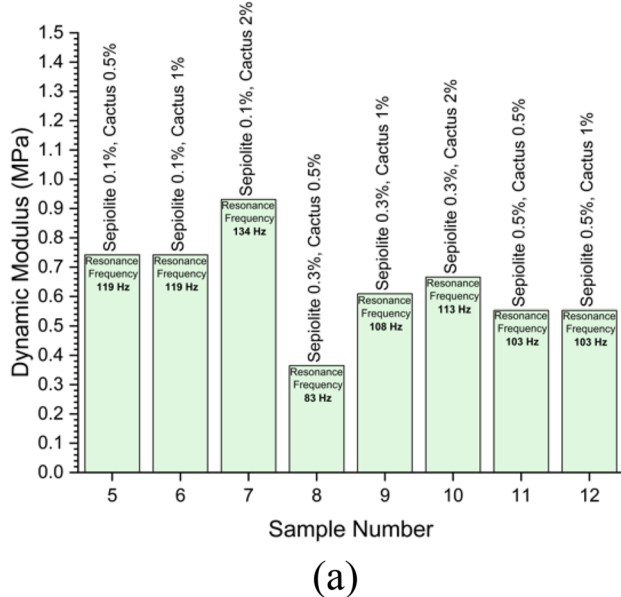


FIG. 7. Maps of (a) dynamic moduli and (b) loss factors measured with the vibration transmissibility tests.

0.55 MPa at 60 °C. Sepiolite particles possess a very high specific surface area with a negative surface potential.³⁷ Accordingly, direct interactions with the carboxylic acid groups on the alginate chains are unlikely; however, accumulation of the Ca₂₊ ions via double layer formation may promote adhesion of the alginate chains to the particle surfaces. In summary, the larger values of storage and loss moduli at temperatures above 30 °C for the sepiolite-based gels indicated the beneficial effect of sepiolite in bonding with the alginate calcium and improving the structural integrity of the gels at different temperatures.

B. Role of the cactus fibers

The incorporation of 1 wt. % of cactus fibers increased the loss modulus of the alginate–poloxamer gels by ~33%. This effect appeared to be temperature-insensitive, although a slightly higher loss modulus was observed at 60 °C. Increasing the weight fractions of cactus fibers enhanced load transfer between the reinforcements and the alginate–poloxamer matrix across all formulations tested in this study (ranging from 0.5 to 2.0 wt. %). Notably, no evidence of fiber clustering was observed with increasing cactus weight fraction, particularly in the vibration transmissibility tests. These findings supported the stiffening effect of low concentrations of cactus fibers, even in comparison to other natural fibers, such as flax and bamboo.¹⁸ Previous studies have attributed this behavior to the multiscale fractal nature of cactus fibers, which induces slip–stick friction effects during dynamic fatigue, thereby increasing energy dissipation of composites.¹⁶ The behavior of the loss modulus (quasi-static and dynamic) also followed a similar trend here, confirming the results obtained from the vibration transmissibility tests carried out on the first generation of alginate–poloxamer–cactus fiber gels with a reinforcement level between 1.25 to 5.0 wt. %.¹⁹

VI. SURROGATE MODELING

The data from the design of experiments for the DMA and the vibration transmissibility tests were used to construct surface response metamodels (SRMs).³⁸ These SRMs are intended to support future optimization of the manufacturing process using machine learning or AI-based techniques by allowing prediction of outcomes based on varying parameters values, in particular the weight fractions of sepiolite and cactus fibers. The SRMs were developed using fifth-order polynomial fittings at three different temperatures (30, 45, and 60 °C) under 20% RH and 1 Hz of excitation. The coefficients of determination (R^2) for the polynomial fits ranged from 0.88 to 0.96, indicating a high level of agreement between the models and experimental data. The coefficients of the fittings for the DMA and the vibration transmissibility tests are provided in [Appendices A](#) and [B](#), respectively ([Tables II–IV](#)). [Figure 8](#) presents the SRMs derived from the data obtained from the DMA tests. These response surfaces indicate that the dispersion of cactus fibers contributes most significantly to variations in loss and storage moduli at a given temperature. In contrast, sepiolite is more effective in enhancing the viscoelastic response at elevated temperature. The most pronounced variations in tan δ are observed at intermediate weight fractions of sepiolite and cactus fibers. [Figure 9](#) and [Table V](#) illustrate the SRMs extracted from the vibration transmissibility test data. The loss moduli in this dataset range from 0.15 to 0.35 MPa, with the highest energy dissipation occurring in

formulations containing at least 2 wt. % cactus fibers. Conversely, the lowest values for both dynamic moduli and resonant frequencies are associated with sepiolite weight fraction exceeding 0.3 wt. %, even when the maximum loading of cactus fibers is used.

VII. CONCLUSIONS

The composite hydrogel materials developed through the design of experiments (DoE) approach in this study demonstrate an increase in quasi-static and storage modulus properties compared to the baseline alginate–poloxamer formulation. The storage modulus values were observed to be up to twice those of the undoped hydrogel, even with highly dilute dispersions of cactus fiber and sepiolite. Sepiolite reinforcements less than 0.3 wt. % were effective in stabilizing and stiffening the gel, particularly at elevated temperature. In contrast, cactus fibers provided a consistent increase in stiffness and damping with increasing weight fractions. These trends were confirmed through both Dynamic Mechanical Analysis (DMA) and vibration transmissibility testing. Notably, high values of loss factors (over ~0.4) during vibration testing were recorded in hydrogels with 0.1 wt. % sepiolite and up to 2 wt. % of cactus fibers. A formulation comprising 5 wt. % alginate, 5 wt. % poloxamer, 0.1 wt. % sepiolite, and 2 wt. % cactus fiber emerged as the optimal configuration, balancing quasi-static stiffness with dynamic performance.

Compared to previous generations of alginate–poloxamer hydrogels,²⁷ the composites developed in this work, particularly those with 0.1 wt. % sepiolite and 2 wt. % cactus fibers, demonstrated up to an order of magnitude increase (0.93 MPa) within the 80–140 Hz frequency range, relative to their static modulus. This is significant as the damping performance of polymers, especially fossil-based ones, is typically suboptimal at low frequencies.⁴ Furthermore, vibration transmissibility tests revealed sensitivity of both loss factors and dynamic moduli to increasing base acceleration (up to 2.5 g¹⁹), suggesting possible granular-type fluidization effects. Similar behaviors have been reported in jammed granular hydrogel systems for bioprinting applications.³⁸ The composite hydrogel (alginate–poloxamer–sepiolite–cactus fiber) also exhibited an average loss modulus around 0.32 MPa, a value that is comparable or exceeding those of conventional damping materials, such as commercial open cell polyurethane foams.²⁸ Remarkably, these improvements were achieved using extremely diluted fiber loadings, matching the relative stiffening effects reported for alginate–PVA-based hydrogels that typically require 10 wt. % reinforcement.¹⁰ Note that the viscoelastic properties in this study were measured under environmental conditions (such as low relative humidity), which can cause dehydration and reduce performance. Thus, further improved results may be expected under more controlled or milder testing conditions. The sepiolite and cactus fiber reinforcements of the hydrogel composites developed in this work have been dispersed using a relative high-speed mixing (2500 rpm). While the technique can yield satisfactory results with diluted dispersions, further improvements in gel composition can be achieved by functionalizing the dispersions. This prevents filler precipitation and enhances homogeneity and cross-linking, such as using hydroxyethyl methacrylate-functionalized nanohydroxyapatite in nanocomposite inks for bioprinting.³⁹

The composite hydrogels developed in this work could be used in tuned vibration damper designs to mitigate low-frequency

vibrations in machinery and reduce vibration transmissibility in electronic packaging containers. Other potential damper designs that could adopt these hydrogels include free and constrained layer dampers, which require layer-by-layer deposition of the damping material to construct the damping device.¹⁹ The biodegradable and bio-based nature of these hydrogel composites offers a promising alternative to fossil materials for designing energy absorption and vibration mitigation solutions.

ACKNOWLEDGMENTS

This work was funded by the UK Defence Science and Technology Laboratory (Grant No. DSTL0000024791), the Office of Naval Research Global (Grant No. N62909-201-2061), and the ERC H2020 AdG NEUROMETA (Project No. 01020715). The authors would also like to express their gratitude to Professor Petra C. Oyston, Mr. Matthew D Eagling (Dstl), Dr. Claire Lonsdale (Dstl), Dr. Dave Hallam (Dstl), Maj. Anthony Kirkham (Dstl), Maj. James Barracough (Dstl), and Dr. Scott A. Walper (ONR G) for their support and insightful discussions throughout the project. The authors also thank Judith Mantell of the Wolfson Bioimaging Facility for their assistance in capturing the Cryo-SEM micrographs presented in this work. The authors would also like to thank Dr Farnaz Ghorbani, Dr. Arpit Nandi, and Professor Martin Kuball for supporting the testing. J.P.K.A. acknowledges funding from a UKRI Future Leaders Fellowship (Grant No. MR/V024965/1).

AUTHOR DECLARATIONS

Conflict of Interest

The authors have no conflicts to disclose.

Author Contributions

Gianni Comandini: Data curation (equal); Formal analysis (equal); Investigation (equal); Methodology (equal); Supervision (equal); Validation (equal); Visualization (equal); Writing – original draft (equal). **Fabrizio Scarpa:** Conceptualization (equal); Formal analysis (equal); Funding acquisition (equal); Investigation (equal); Project administration (lead); Writing – review & editing (lead). **Evita Ning:** Formal analysis (equal); Investigation (equal); Methodology (equal); Validation (equal); Writing – review & editing (supporting). **Graham J. Day:** Conceptualization (equal); Methodology (equal); Resources (equal); Validation (equal); Writing – review & editing (supporting). **Hesam Ramezani:** Formal analysis (supporting); Investigation (supporting). **James P. K. Armstrong:** Formal analysis (equal); Investigation (equal); Methodology (equal); Supervision (equal); Writing – review & editing (supporting). **Abderrezak Bezazi:** Conceptualization (equal); Resources (equal); Validation (supporting). **Adam W. Perriman:** Conceptualization (equal); Funding acquisition (equal); Methodology (equal); Supervision (equal); Validation (equal).

DATA AVAILABILITY

The data that support the findings of this study are available within the article.

APPENDIX A: SURFACE RESPONSE FROM THE DMA TESTS

Surface responses at different temperatures for (a) loss moduli, (b) storage moduli, and (c) tan δ.

TABLE II. Coefficients for the storage, loss moduli, and tan δ of the DMA tests at 30 °C.

Equation term	Coefficient	Loss modulus (Mpa) R^2=0.9665	Storage modulus (Mpa) R^2=0.9201	Tan δ R^2=0.9366
x1=Sepiolite wt% x2=Cactus fibres wt%				
x1	a0	0.232	1.1428	0.1907
x2	a1	-0.2536	-0.9659	0.0452
x2 ^2	a2	0	0	0
x2 ^3	a3	0.6667	2.8487	-0.0538
x2 ^4	a4	-0.3051	-1.3239	0
x2 ^5	a5	0	0	0.0114
x1	a6	0.228	3.31	0.0956
x1 * x2	a7	1.6098	4.8187	-3.5844
x1 * x2 ^2	a8	-1.6846	-8.3329	3.7688
x1 * x2 ^3	a9	0.6388	3.6014	0
x1 * x2 ^4	a10	0	0	-0.4949
x1 ^2	a11	-0.7646	-24.216	1.6046
x1 ^2 * x2	a12	-4.3118	-6.8573	13.6485
x1 ^2 * x2 ^2	a13	-0.0364	-2.6024	-13.4238
x1 ^2 * x2 ^3	a14	0	0	3.144
x1 ^3	a15	0.6775	33.593	-2.9619
x1 ^3 * x2	a16	5.8941	16.6323	-12.8924
x1 ^3 * x2 ^2	a17	0	0	6.9039

TABLE III. Coefficients for the storage, loss moduli, and tan δ of the DMA tests at 45 °C.

Equation term	Coefficient	Loss modulus (Mpa) R^2=0.9351	Storage modulus (Mpa) R^2=0.9525	Tan δ R^2=0.9538
x1=Sepiolite wt% x2=Cactus fibres wt%				
x2	a0	0.2352	1.0785	0.207
x2	a1	-0.3089	-1.0883	0.0126
x2^2	a2	0	0	0
x2^3	a3	0.7707	2.9645	-0.0073
x2^4	a4	-0.3487	-1.3568	0
x2^5	a5	0	0	0.0015
x1	a6	-0.0175	2.2946	-0.0584
x1 * x2	a7	2.4919	7.4902	-2.2066
x1 * x2^2	a8	-2.0973	-8.5185	2.3472
x1 * x2^3	a9	0.688	3.1685	0
x1 * x2^4	a10	0	0	-0.2968
x1^2	a11	1.2099	-14.3866	2.0191
x1^2 * x2	a12	-6.9773	-16.9131	8.7806
x1^2 * x2^2	a13	0.4964	-0.0482	-8.7984
x1^2 * x2^3	a14	0	0	1.9502
x1^3	a15	-2.2601	18.6535	-3.2792
x1^3 * x2	a16	7.9233	23.1414	-8.7815
x1^3 * x2^2	a17	0	0	5.0332

TABLE IV. Coefficients for the storage, loss moduli, and tan δ of the DMA tests at 60 °C.

Equation term	Coefficient	Loss modulus (Mpa) R^2=0.9655	Storage modulus (Mpa) R^2=0.9679	Tan δ R^2=0.9655
x1=Sepiolite wt% x2=Cactus fibres wt%				
x2	a0	0.2922	1.135	0.2562
x2	a1	-0.4458	-1.3099	-0.0785
x2^2	a2	0	0	0
x2^3	a3	1.1167	3.4154	0.1543
x2^4	a4	-0.5062	-1.5561	-0.0677
x2^5	a5	0	0	
x1	a6	-0.6846	0.8755	-0.6084
x1 * x2	a7	3.7714	9.0364	0.9461
x1 * x2^2	a8	-2.1089	-6.5741	-0.3795
x1 * x2^3	a9	0.9677	3.249	0.0685
x1 * x2^4	a10	0	0	0
x1^2	a11	13.2573	17.7026	5.0561
x1^2 * x2	a12	-20.5686	-49.2297	-3.9291
x1^2 * x2^2	a13	-0.7943	-3.9052	0.5038
x1^2 * x2^3	a14	0	0	0
x1^3	a15	-23.2146	-37.9938	-7.2317
x1^3 * x2	a16	30.5701	79.2606	3.726
x1^3 * x2^2	a17	0	0	0

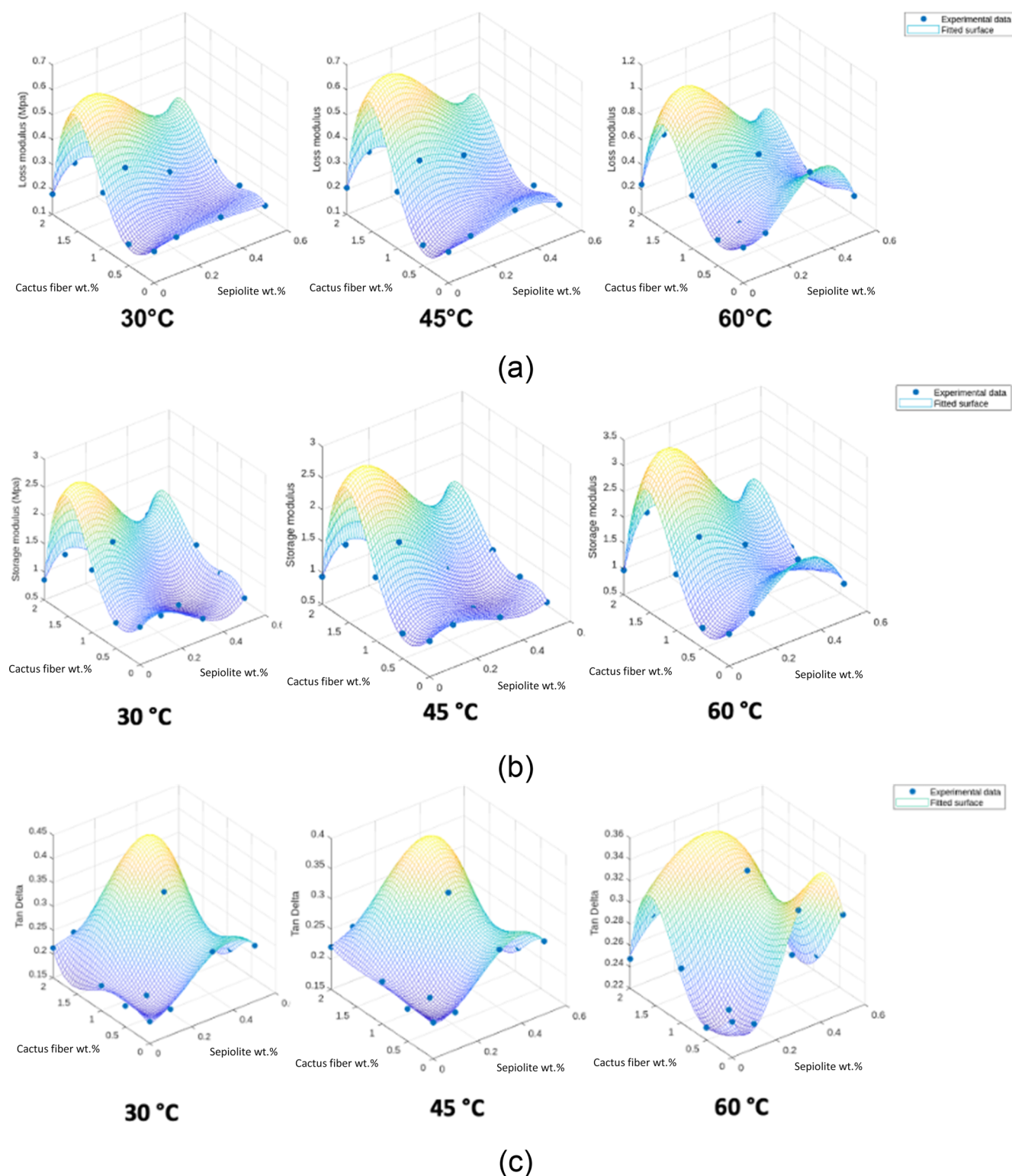


FIG. 8. Surface responses at different temperatures for (a) loss moduli, (b) storage moduli, and (c) tan δ .

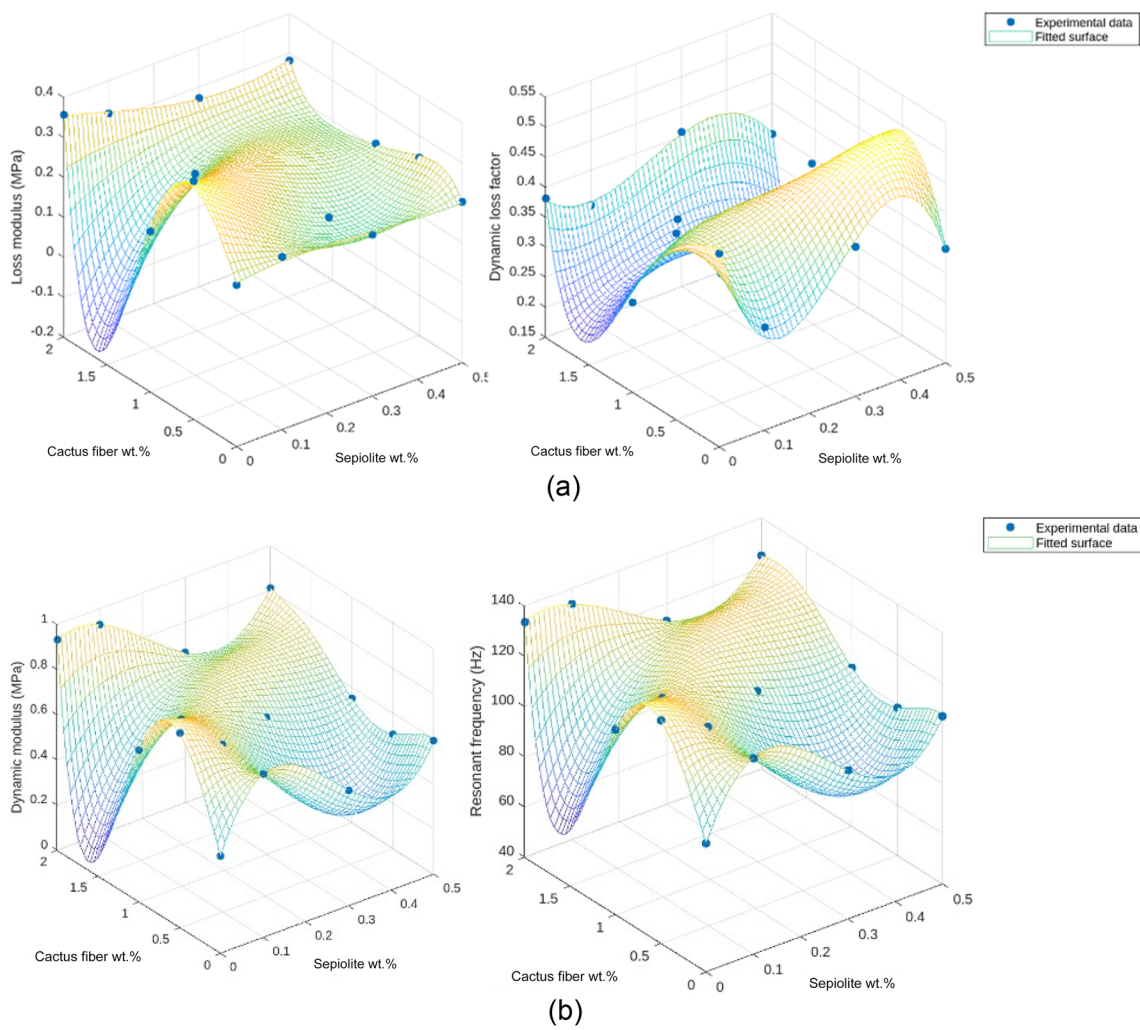


FIG. 9. Surface response models for (a) loss modulus and dynamic loss factors and (b) dynamic modulus and resonant frequencies for the data related to the composite hydrogels measured using the vibration transmissibility tests.

TABLE V. Coefficients of the SRMs for the dynamic modulus, loss modulus, and resonant frequencies.

Equation term	Coefficient	Dynamic modulus (Mpa) R^2=0.9999	Dynamic loss factor R^2=0.8851	Loss modulus (Mpa) R^2=0.9544	Resonant frequency (Hz) R^2=0.9998
x1=Sepiolite wt%	x2=Cactus fibres wt%	a0	0.4329	0.4816	0.2103
x2	a1	1.1151	-0.0571	0.4851	98.191
x2^2	a2	0	0	0	0
x2^3	a3	-1.0931	-0.1428	-0.6078	-94.6437
x2^4	a4	0	0	0	0
x2^5	a5	0.2192	0.036	0.1261	18.8561
x1	a6	5.2252	-3.1219	0.2016	487.1795
x1 * x2	a7	-20.4426	6.1747	-5.4617	-1863.8346
x1 * x2^2	a8	19.094	-2.0875	7.7134	1734.7081
x1 * x2^3	a9	0	0	0	0
x1 * x2^4	a10	-2.4843	-0.0994	-1.2776	-226.2982
x1^2	a11	-26.5872	15.5565	-0.9501	-2467.8144
x1^2 * x2	a12	56.4367	-29.1862	5.418	5109.1376
x1^2 * x2^2	a13	-52.1447	9.1966	-17.6422	-4707.8775
x1^2 * x2^3	a14	13.803	1.3387	7.549	1268.4255
x1^3	a15	33.5585	-19.7863	1.0076	3112.9735
x1^3 * x2	a16	-38.9232	39.4368	10.8457	-3440.0568
x1^3 * x2^2	a17	15.797	-16.4585	-5.3613	1313.447

APPENDIX B: COEFFICIENTS OF THE SURFACE RESPONSE FROM THE VIBRATION TRANSMISSIBILITY TESTS

Surface response models for (a) loss modulus and dynamic loss factors and (b) dynamic modulus and resonant frequencies for the data related to the composite hydrogels measured using the vibration transmissibility tests.

REFERENCES

- ¹J. William Strutt and B. Rayleigh, *The Theory of Sound* (MacMillan and Co., London, 1877).
- ²R. E. D. Bishop, *J. R. Aeronaut. Soc.* **59**(539), 738 (1955).
- ³H. Kolsky, *Philos. Mag.* **1**(8), 693 (1956).
- ⁴D. I. G. Jones, *Handbook of Viscoelastic Vibration Damping* (John Wiley & Sons Ltd, 2001).
- ⁵R. Plunkett, in *M3D: Mechanics and Mechanisms of Material Damping*, edited by V. K. Kinra and A. Wolfenden (ASTM International, 1992), Vol. STP1169-EB.
- ⁶R. Lakes, *Viscoelastic Solids* (CRC Press, Boca Raton, FL, 1998).
- ⁷R. Plunkett, “Damping analysis: An historical perspective,” in *M3D: Mechanics and Mechanisms of Material Damping*, edited by V. K. Kinra and A. Wolfenden (ASTM International, 1992), Vol. STP1169-EB, p. 0.
- ⁸T. Liu, P. Butaud, P. Vincent, and M. Ouisse, *Comp. Struct.* **275**, 114392 (2021).
- ⁹C. Lim, Y. Shin, J. Jung, Ji H. Kim, S. Lee, and D.-H. Kim, *APL Mater.* **7**(3), 031502 (2018); X. Liu, Y. Hu, Y. Ju, P. Yang, N. Shen, A. Yang, R. Wu, B. Fang, and L. Liu, *APL Mater.* **12**(8), 080603 (2024).
- ¹⁰X. Du, Y. Zhou, D. Schümperlin, L. Laganenka, S. S. Lee, G. Blugan, W.-D. Hardt, C. Persson, and S. J. Ferguson, *J. Mech. Behav. Biomed. Mater.* **155**, 106579 (2024).
- ¹¹J. Li, Y. Yang, H. Jiang, Y. Wang, Y. Chen, S. Jiang, J.-M. Wu, and G. Zhang, *Composites, Part B* **232**, 109617 (2022).
- ¹²B. Wang, A. G. Moura, J. Chen, A. Erturk, and Y. Hu, *Extreme Mech. Lett.* **40**, 100841 (2020).
- ¹³W. Lu, Q. Zhang, F. Qin, P. Xu, Q. Chen, H. Wang, F. Scarpa, and H.-X. Peng, *Appl. Mater. Today* **25**, 101222 (2021).
- ¹⁴S. A. A. X. Michel, R. R. M. Vogels, N. D. Bouvy, M. L. W. Knetsch, N. M. S. van den Akker, M. J. J. Gijbels, C. van der Marel, J. Vermeersch, D. G. M. Molin, and L. H. Koole, *J. Biomed. Mater. Res., Part B* **102**(3), 477 (2014); C. de Kergariou, G. J. Day, A. W. Perriman, J. P. K. Armstrong, and F. Scarpa, *Soft Matter* **20** (19), 4021 (2024).
- ¹⁵L. Rakowitz, *Rangelands* **19**(6), 15 (1997).
- ¹⁶M. Bouakba, A. Bezazi, K. Boba, F. Scarpa, and S. Bellamy, *Compos. Sci. Technol.* **74**, 150 (2013).
- ¹⁷A. Hetherington, I. Zampetakis, A. Perriman, and F. Scarpa, in *18th European Conference on Composite Materials, ECCM 2018* (Applied Mechanics Laboratory, Athens, Greece, 2018).
- ¹⁸I. Zampetakis, “Cactus based solids,” Ph.D. thesis, University of Bristol, 2021. <https://hdl.handle.net/1983/2c57a54f-2c3e-4313-8c2b-71a41bc42dba>
- ¹⁹F. D. Scarpa, G. J. Perriman, and A. Willis, “A composite hydrogel composition,” UK Intellectual Property Office Patent Application 2405258.1 (filed 04/12/2024).
- ²⁰B. F. Jones and K. M. Conko, *Dev. Clay Sci.* **3**, 69 (2011).
- ²¹W. Ji, Q. Zhang, F. Alvarez-Borges, G. Yuan, J. Van Duijneveldt, W. H. Briscoe, and F. Scarpa, *Compos. Struct.* **322**, 117419 (2023).
- ²²W. Ji, Q. Zhang, J. S. van Duijneveldt, W. H. Briscoe, and F. Scarpa, *ACS Appl. Polym. Mater.* **6**, 010322 (2024).
- ²³S. Ekici, Y. İşikver, and D. Saraydin, *Polym. Bull.* **57**(2), 231 (2006).
- ²⁴Y. Jiang, L. Wang, W. Qi, P. Yin, X. Liao, Y. Luo, and Y. Ding, *Biomater. Adv.* **159**, 213838 (2024).
- ²⁵Y. Jiang, S. Wen, S. Lin, D. Jin, and Y. Ding, *ChemistrySelect* **9**(24), e202401210 (2024).
- ²⁶J. E. Martín-Alfonso, M. J. Martín-Alfonso, and J. M. Franco, *Appl. Clay Sci.* **192**, 105632 (2020).
- ²⁷G. J. Day, Q. Zhang, C. D. L. Remillat, G. Comandini, A. W. Perriman, and F. Scarpa, *Commun. Mater.* **6**(1), 148 (2025).
- ²⁸Q. Zhang, X. Yu, F. Scarpa, D. Barton, Y. Zhu, Z.-Q. Lang, and D. Zhang, *Mech. Syst. Signal Process.* **179**, 109375 (2022).
- ²⁹C. Narayan and M. N. Das Giri, *Design and Analysis of Experiments* (Wiley, New York, 1976).
- ³⁰M. Zou, H. Guo, Q. Zhang, H. Wang, Z. Ji, C. Margadji, K. Samson, A. Kuswoyo, F. Scarpa, M. Saed, and S. W. Pattinson, *Appl. Mater. Today* **40**, 102396 (2024).
- ³¹E. Peña, J. A. Peña, and M. Doblaré, *Int. J. Solids Struct.* **46**(7), 1727 (2009).
- ³²G. Lawrie, I. Keen, B. Drew, A. Chandler-Temple, L. Rintoul, P. Fredericks, and L. Grøndahl, *Biomacromolecules* **8**(8), 2533 (2007); Q. Xiao, X. Gu, and S. Tan, *Food Chem.* **164**, 179 (2014).
- ³³I. Popescu, M. Turtoi, D. M. Suflet, M. V. Dinu, R. N. Darie-Nita, M. Anghelache, M. Calin, and M. Constantin, *Int. J. Biol. Macromol.* **180**, 418 (2021); Y. Kim, M.-K. Yoo, B.-C. Kim, S.-K. Kim, H.-C. Lee, and C.-S. Cho, *Int. J. Biol. Macromol.* **38** (1), 51 (2006).
- ³⁴T. Perraki and A. Orfanoudaki, *J. Therm. Anal. Calorim.* **91**(2), 589 (2008); Y. Turhan, P. Turan, M. Doğan, M. Alkan, H. Namli, and Ö. Demirbaş, *Ind. Eng. Chem. Res.* **47** (6), 1883 (2008).
- ³⁵M. A. Wahab, H. Boubakri, S. Jellali, and N. Jedidi, *J. Hazard. Mater.* **241–242**, 101 (2012); M. Cheikh Rouhou, S. Douiri, S. Abdelmoumen, A. Ghorbal, A. Lung, C. Raynaud, and D. Ghorbel, *Anal. Biochem.* **670**, 115139 (2023).
- ³⁶Y. Luo, S. Xiong, J. Huang, F. Zhang, C. Li, Y. Min, R. Peng, and Y. Liu, *Sol. Energy Mater. Sol. Cells* **231**, 111300 (2021).
- ³⁷W. Jiang, Y. Jiang, S. Zhao, J. Peng, W. Qin, D. Ouyang, and Y. Ding, *Energy Technol.* **8**(3), 1901262 (2020).
- ³⁸L. Riley, L. Schirmer, and T. Segura, *Curr. Opin. Biotechnol.* **60**, 1 (2019).
- ³⁹Y. Yang, Q. Zhang, T. Xu, H. Zhang, M. Zhang, L. Lu, Y. Hao, J. H. Fuh, and X. Zhao, *Biomaterials* **263**, 120378 (2020).